Properties of Nanocrystals-formulated Aluminosilicate Bricks

Regular Paper

Francesca Conciauro[1], Emanuela Filippo[1], Claudia Carlucci[2], Viviana Vergaro[3], Francesca Baldassarre[3], Rosaria D'Amato[4], Gaetano Terranova[4], Caterina Lorusso[1], Paolo Maria Congedo[1], Barbara Federica Scremin[3] and Giuseppe Ciccarella[1,3]*

1 Department of Innovation Engineering-University of Salento, Lecce, Italy
2 Chemistry Department, University of Bari, Bari, Italy
3 CNR NANOTEC - Institute of Nanotechnology of the National Research Council, c/o Campus Ecotekne, University of Salento, Lecce, Italy
4 ENEA Frascati Research Centre, Frascati Roma, Italy
*Corresponding author(s) E-mail: giuseppe.ciccarella@unisalento.it

Abstract

In the present work, seven different types of nanocrystals were studied as additives in the formulation of aluminosilicate bricks. The considered nanocrystals consisted of anatase titanium dioxide (two differently shaped types), boron modified anatase, calcium carbonate (in calcite phase), aluminium hydroxide and silicon carbide (of two diverse sizes), which were prepared using different methods. Syntheses aim to give a good control over a particle's size and shape. Anatase titania nanocrystals, together with the nano-aluminium hydroxide ones, were synthesized via microwave-assisted procedures, with the use of different additives and without the final calcination steps. The silicon carbide nanoparticles were prepared via laser pyrolysis. The nano-calcium carbonate was prepared via a spray drying technique. All of the nanocrystals were tested as fillers (in 0.5, 1 and 2 wt. % amounts) in a commercial aluminosilicate refractory ($55\% Al_2O_3$, $42\% SiO_2$). They were used to prepare bricks that were thermally treated at 1300 °C for 24 hours, according to the international norms. The differently synthesized nanocrystals were added for the preparation of the bricks, with the aim to improve their heat-insulating and/or mechanical properties. The nanocrystals-modified refractories showed variations in properties, with respect to the untreated aluminosilicate reference in heat-insulating performances (thermal diffusivities were measured by the "hot disk" technique). In general, they also showed improvements in mechanical compression resistance for all of the samples at 2 wt. %. The best heat insulation was obtained with the addition of nano-aluminium hydroxide at 2 wt. %, while the highest mechanical compression breaking resistance was found with nano-$CaCO_3$ at 2 wt. %. These outcomes were investigated with complementary techniques, like mercury porosimetry for porosity, and Archimedes methods to measure physical properties like the bulk and apparent densities, apparent porosities and water absorption. The results show that the nano-aluminium hydroxide modified bricks were the most porous, which could explain the best heat-insulating performances. There is a less straightforward explanation for the mechanical resistance results, as they may have relations with the characteristics of the pores. Furthermore, the nanoparticles may have possible reactions with the matrix during the heat treatments.

---

1. Introduction

The development of new heat-insulating materials is an important technological innovation factor. In the last decade, building refractories have emerged as an important industrial sector [1]. In particular, this development concerns the improvement of thermo-physical properties through the identification of ad hoc formulations [2-5]. Indeed, on the market, new products compete against each other for the parameters that characterize the performances of refractories. At first, such products focused on less thermal diffusivity, a better porosity distribution, a better thermal shock, acid environments and high temperature mechanical resistance. For these reasons, a product showing improved performances would find commercial industrial spaces especially in the iron and steel industrial sector. In this sector, continuous research is being carried out about new refractory materials that are able to work at high temperatures, in corrosive atmospheres and under mechanical stress. From an industrial perspective, the advantage of employing new performing materials implies a longer life of plants and less maintenance requests. The thermal behaviour of a refractory material falls in the field of interest of many engineering problems like cooling processes, thermal insulation, and mechanical and high temperature resistance. In general, non-metallic materials are thermal insulators since their electrons are involved in a structural covalent or ionic bonds. In the case of refractory materials, lattice vibrations are responsible for heat transfer. This is because their energy gap between valence and conduction bands is too wide, and valence electron promotion into the conduction band may eventually only be possible at very high temperatures. Some materials at high temperatures have thermal conductivity values that are high, whilst others conduct less heat. Many factors may influence thermal conductivity in non-metallic materials: a packed structure, a low density and a high elastic modulus produce high-energy electrons, which favour heat transmission. Therefore, crystalline solids have a higher thermal conductivity with respect to their amorphous or vitreous counterparts.

Aluminosilicate refractories are refractory clay mixtures with an alumina content (generally between 20 and 40 %) and a lighter material (quartz or chamotte). "Chamotte" is a refractory clay that is made of an alumina Al_2O_3 and amorphous silica SiO_2 mixture.

The present research work aims to study and develop high thermal capacity and low thermal conductivity nanocrystals-modified refractories, which are suitable for plant coating in the iron and steel industry.

One of remarkable nanocrystals properties is a high surface/volume atomic ratio, which influences the macroscopic features of a composite material. Indeed, one of the difficulties in working with nanocrystals is to overcome their tendency to aggregate into micrometric crystalline forms, which reduce their surface free energy. Therefore, it is important that the nano-fillers are uniformly dispersed in the matrix and that they present the same shape, size and composition to successfully concur to the final properties of the composite.

In this paper, we present the investigation results that were carried out on nanocrystals-formulated aluminosilicates. These were prepared from "chamotte" and different suspensions of nanocrystals in benzyl alcohol were added. The nanocrystals were synthesized in different ways - in particular, surfactant free and without the requirement of the final calcination steps. Seven nanocrystal types were investigated: nano-aluminium hydroxide (nano-$Al(OH)_3$); three kinds of nano-anatase titania (TiO_2-NS–nanospheres, TiO_2-NR nanorods and boron-modified TiO_2-B); two nano-silicon carbide (nano-SiC) and nano-calcium carbonate (nano-$CaCO_3$). Three different concentrations (0.5 wt. %, 1 wt. % and 2 wt. %) of nanocrystals in the aluminosilicate matrix were explored versus the reference commercial material, since there was no literature or specific protocol prescriptions. The reference brick was prepared directly from the commercial material (Vibrec 545 F) without further additives. All of the bricks were thermally treated at 1300 °C, according to the international norms. The thermal treatment of the bricks at 1300 °C may have changed the nanocrystals from their initial state. However, we studied the properties of the final product. Finally, the physical properties (thermal diffusivity, porosity, density and water absorption), together with the mechanical properties (compression resistance), were comparatively studied.

In particular, porosity is an important microstructural characteristic: energy and mass transport phenomena, compression mechanical resistances, scrape and deterioration resistances are related to the amount of voids, their shape and linking, and their size distribution. In order to understand the material's macroscopic characteristics, voids are not less important than the chemical and mineralogical composition. In ceramic materials, porosity is closely related to the sizes of the particles that are used for their preparation and with the characteristics of the sintering process. In refractory materials, porosity depends on the particle size of the solid phases, as well as the water to cement ratio, the hydration degree and the ageing time. Even when it is high, porosity should not be considered negatively. Compression resistance is certainly influenced by the empty space as a function of less resistant areas and of the presence of stress concentrators. However, there are other properties, such as energy transport and thermal insulation, which are positively related to a porous structure.

2. Materials and Methods

2.1 Syntheses of the Nanocrystals

Seven kind of nanocrystals were synthesized using different techniques and reaction conditions: nano-aluminium hydroxide $Al(OH)_3$; and three kinds of nano-anatase titania TiO_2–nanospheres (TiO_2-NS [6], TiO_2-NR nanorods [7] and boron-modified TiO_2-B) [8] by microwave-assisted syntheses; nano-silicon carbide SiC by laser pyrolysis [9], and nano-calcium carbonate $CaCO_3$ by spray drying [10]. In the following sections, the procedures are presented in more detail.

Generally, all of the microwave-assisted nanocrystal syntheses of the present study were conducted using a microwave digestion system (model Mars, CEM, Matthews, NC). The system used a 2.45 GHz microwave frequency and was controlled by both temperature (set according to the specific case, typically 150-200 °C) and pressure (300 psi for all of the nanocrystals). The reaction Teflon vessel line (XP 1500) was connected to a pressure transducer, which monitored and controlled the pressure during the synthesis. Next, the vessel was sealed and maintained at the chosen temperature and time, under magnetic stirring. The resulting suspensions were collected by centrifugation and washed thoroughly by the chosen solvent. They were finally dried under the desired conditions (generally, under vacuum at 50 °C for 6 h or dried overnight at ambient temperature), without the post-synthetic calcination treatment of the nanocrystals [11].

The nano-aluminium hydroxide $Al(OH)_3$ was synthesized via a microwave-assisted procedure. In our samples, 0.686 g (3.36 mmol) of $Al(iPrO)_3$, aluminium triidropropoxide was dissolved into 10 ml of benzyl alcohol in a Teflon vessel. Successively, to obtain a $Al(iPrO)_3$: acetic acid ratio of 1:5, 0.97 ml (16.8 mmol) acetic acid was added in the vessel and then sealed. The reaction was carried out at 150 °C for 60 minutes under magnetic stirring. Subsequently, the product was collected by centrifugation at 30000 rpm for 15 min and washed three times (using the same centrifugation conditions) with methanol. It was then dried overnight at ambient temperature.

The TiO_2 nanospheres [6] and nanorods [7] were prepared via a non-aqueous method - a microwave-assisted synthesis with the reaction of titanium tetraisopropoxide $Ti(iPrO)_4$ (TTIP) in benzyl alcohol in presence of acetic acid (nanospheres) or oleic acid (nanorods). In the procedure, 1 ml (3.36 mmol) of TTIP was slowly added to 10 ml of benzyl alcohol in a Teflon® vessel. Aacetic acid or oleic acid were successfully added dropwise. The vessel was then sealed and kept at 210 °C for 45 min under magnetic stirring. Subsequently, the product was collected by centrifugation at 30000 rpm for 15 min and washed three times (using the same centrifugation conditions) with methanol. It was then dried overnight at ambient temperature. The tested nanospheres were prepared with a ratio TTIP: acetic acid of 1:2 (0.32 ml, 6.72 mmol of acetic acid), or TTIP: oleic acid of 1:2 (8.6 ml, 26.8 mmol).

The boron modified anatase titania nanocrystals [8] were prepared using the reaction of TTIP in the presence of benzyl alcohol as a reaction solvent with the addition of boric acid via a microwave-assisted synthesis. In the procedure, 1 ml (3.36 mmol) of TTIP was slowly added to 10 ml of benzyl alcohol in a Teflon vessel. Boric acid (TTIP: boric acid 1:1 molar ratio) was successively added. The vessel was then sealed and kept at 150 °C for 1 and a half min under magnetic stirring. The microwave-assisted synthesis took place in a single and fast reaction step. The product was collected by centrifugation (30000 rpm, 15 min) and washed three times with dichloromethane (collected using the centrifuge 30000 rpm, 15 min). It was then dried overnight at ambient temperature.

The nano-silicon carbide SiC was prepared via laser pyrolysis [9], starting from two gaseous reagents, silane SiH_4 and acetylene C_2H_2. Laser pyrolysis, which is classified as a vapour-phase synthesis of nanoparticles (NPs), permitted highly localized and fast heating (leading to a rapid nucleation) in a volume that could be limited to a few hundred mm^3, followed by a fast quenching of the particle growth (in a few msec). As a result, the NPs, which had an average size ranging from 5 to 60 nm and narrow size distribution, were formed in the hot region. The mean size of the NPs could have been varied by acting on the process parameters such as the residence time of the particles in the flame, the total pressure in the reaction chamber and the reaction temperature. In this specific case, the set-up for the production of SiC NPs [9] used a CO_2 laser beam ($\lambda = 10.6$ μm), which was focused by a spherical lens (focal length F. L. 12 or 19 cm) at the centre of a reaction chamber (volume V~ 6.8×10^{-3} m^3). Here, it intersected the reactant gas flow orthogonally. The laser power that was used for the present synthesis was 630 W. The reactant gases were injected into the chamber in molar proportion SiH_4: C_2H_2 of 2:1 (through the use of flow controllers, to produce pure SiC) via an inner tube of a coaxial stainless steel nozzle with either a diameter of 3 or 6 mm. The inert gas Ar flowed at 5 standard litres per minute (slm) through the outer tube with the purpose of confining and cooling the particles. The pressure in the reaction chamber was kept constant at 8.0×10^4 Pa and measured by a pressure control unit. The acetylene flow was set at 250 standard cubic centimetres per minute (SCCM). SiC-16 was obtained with F.L. of 12 cm, a nozzle diameter of 3 mm and a SiH_4 flux of 300 SCCM, while SiC-28 with F.L. of 19 cm, nozzle diameter of 6 mm and a SiH_4 flux of 500 SCCM. [9]

The nano-calcium carbonate $CaCO_3$ in calcite phase was synthesized by a spray drying technique [10]. With this technique, the use of surfactant additives or other chemical species for the stabilization of a reaction mixture is avoided. The parameters that were under control for the atomization process modulation were temperature and the reactants'

fluxes. The reactants that were used were $NaHCO_3$ and $CaCl_2$ in molar ratios 2:1.

Specifically, 250 ml of 0.011 g/ml $NaHCO_3$ aqueous solution was mixed with 250 ml of $CaCl_2$ 0.009 g/ml immediately before the vaporization stage at 140 °C. Two peristaltic pumps controlled the solutions' fluxes. The high temperature, due to water evaporation from the reaction mixture, allowed the direct production of the calcium carbonate powders, which accumulated in the collecting beaker. The side that produced NaCl was dissolved by the subsequent water washings. The carrier air flux was set at 60 m³/s. The obtained nanoparticles were uniformly dispersed in size and did not form aggregates.

All of the chemicals were analytical-grade reagents and used without further purification.

2.2 Preparation of the Aluminosilicate Bricks

The aluminosilicate material that was used as a composite matrix in the present investigation was a commercial refractory with 5 mm particle size. This was principally made of 55 % alumina and 42 % silica, named Vibrec 545 F.

According to the UNI EN 196/2005 [11], the parallelepiped bricks (160 x 40 x 40 mm in size) were prepared to study their thermo-physical and mechanical parameters.

The nanocrystals were tested as fillers dispersed into the matrix. They were prepared in three different suspensions of benzyl alcohol (then nanocrystals agglomeration was avoided) in concentration percentages of 0.5 wt. %, 1 wt. % and 2 wt. %, respectively. The bricks were obtained mixing 2.2 kg of the commercial matrix refractory material with 6 wt. % of water, in which the additive suspensions were previously mixed. The mixture was added to the mould in two different steps, spaced by a compaction process (carried on with a shaking table, where 60 shaking beats were applied in total). Successively, the bricks where placed in a curing chamber at 20 °C and exposed to no less than 90 % of relative humidity for 24 hours. Each brick was then carried out of the mould and put back in the chamber to mature for 28 days, as described in UNI EN 196/2005 [11]. Later, all of the specimens were fired at 1300 °C for 24 hours.

2.3 Characterization of the Nanocrystals

The morphology of $Al(OH)_3$, TiO_2 (spheres, rods and boron modified) and $CaCO_3$ nanocrystals was studied by transmission electron microscopy (TEM) with a Jeol Jem 1011. TiO_2 [6, 7, 8] and $CaCO_3$ [10] nanocrystals phases were detected by X-Ray Diffraction (XRD) and Raman microscopy. XRD was performed by a Rigaku RINT2500 diffractometer, using a Cu Kα monochromatic radiation (λ = 1.5418 Å). The XRD patterns were recorded in the range of $2\theta = 20°–90°$ by a coupled $\theta/2\theta$ scanning mode, using 2θ increments of 0.03°. The XRD patterns were analysed using a whole-profile Rietveld-based fitting program [12] [6, 7,

8]. $Al(OH)_3$ acetate was recognized from the XRD patterns. A Raman microscopy was accomplished with a Renishaw inVia Raman microscope, with an edge filtered working at a 633 nm excitation wavelength. The powders of the prepared samples were placed on a glass slide and spectra were collected at room temperature. The power on the samples was around 0.8 mW, under a 50X microscope objective, giving a spot diameter of 2 μm, and a resolution of 4 cm⁻¹ was used. The boron modified nanocrystals [13] were characterized by the boron amount using an Inductively Coupled Plasma-Atomic Emission Spectroscopy (ICP-AES). This was performed on a Varian Vista AX ICP-AES instrument with samples that were digested using a mixture of HNO_3 and HF 1:1. The ICP-AES measurements were calibrated using aqueous standards of Ti and B after appropriate dilution. The calibration ranges were selected according to the expected concentrations of the elements of interest. The SiC nanocrystals [9] were characterized by XRD and its morphology was studied using a scanning electron microscopy (SEM) with a Zeiss FEG-SEM LEO 1530. This was equipped with an in-lens secondary electron detector, a conventional secondary electron detector and a scintillation Centaurus detector for backscattered electrons in order to investigate the nanoparticles diameters and their polydispersion.

2.4 Characterization of the Aluminosilicate Bricks

All of the thermal, physical, mechanical and morphological properties of the bricks were characterized using different techniques. The tests were carried out on bricks that were prepared with the three different percentages of nano-fillers, as well as on an unmodified brick. After being thermally treated at 1300 °C for 24 hours or simply dried at 150°C for 5 hours, the nanocrystals-unmodified reference bricks were tested and compared. The nanocrystals-modified bricks were thermally treated at 1300 °C, according to the international norms and tested comparatively with the corresponding reference brick.

2.4.1 Heat Transfer Properties

The heat transfer properties were studied using the hot disk technique [14]. This technique allows the thermal conductivity measure of a wide range of materials (solids, liquids, powders, pastes and foams) with different shapes and sizes (thin films, coatings or adhesive layers, sheets, anisotropic or multi levels samples). The hot disk technique uses the Transient Plane Source (TPS) method [15], which is the generation of heat over a plane under transient conditions. This is possible thanks to a sensor in the form of a thin metallic nickel stripe, wound in a double spiral on a flat support. The spiral is enclosed between two Kapton printed layers over it. Kapton is a poor electrical conductor material but an exceptional heat conductor. This disk is applied on a face of the sample under testing. The hot disk

apparatus uses software for tests and an analysis and automatically controls the temperature of external devices.

In the present work, the thermal conductivity measurements were performed with a hot disk thermal constant analyser (Hot Disk TPS 2500 S 6.1). The brick samples were conditioned at equilibrium with external ambient (T = 20 °C). They were then inserted in the apparatus in contact with the Kapton coated disk sensor (radius 9.869 mm), which constituted the source of thermal power, set at 350 mW for 40 seconds. The generated heat, which dissipated from the sensor into the surrounding unknown sample material, caused a temperature variation both in the sensor and in the surrounding material. In summary, the disk sensor was placed between two pieces of the sample material and then heated by a constant electrical current for about 40 s. The sensor average transient temperature was simultaneously measured, monitoring a change in its electrical resistance. The sensor resistivity change was correlated with the corresponding change in temperature through a temperature coefficient of resistivity. In particular, thermal diffusivity was evaluated.

2.4.2 *The Apparent and Bulk Density, Water Absorption and Apparent Porosity*

The apparent and bulk density, water absorption and apparent porosity of bricks were determined via the Archimedes method. This uses water as the liquid, in conformity with the international ASTM C 20 [16] regulations.

2.4.3 *The Refractory Mechanical Performances*

The refractory mechanical performances were estimated using compression breaking tests, according to the standard in force (UNI EN 196/2005) [11]. Prismatic specimens (4 x 4 x 4 cm) were used and a 65-L12G2 Controls programmed control press was employed. The load was increased uniformly at a speed of 2400 N / s until specimen failure, which is of the brittle type. The tests were performed in triplicate for each sample and the mean values were reported.

2.4.4 *Pore Distribution and Size*

The pore distribution and size of the refractory materials were considered. The porosimetry [17] measurements were achieved using a Pascal 140 and 240 Thermo Finnigan mercury porosimeters. This technique allows the pore size and volumes to be measured through the mercury penetration in the sample open porosity. Mercury is a non-wetting liquid towards a wide range of materials. This technique is applied whenever a material does not contain metals (as Au or Al) that can react with the mercury. Mercury is forced to penetrate the pores by gradually increasing the applied pressure. Initially, when a dilatom-

eter is filled with mercury under vacuum conditions, the mercury surrounds the sample without penetrating it. This is because of the low residual pressure. Then, the pressure is ramped progressively and the penetrated mercury volume is simultaneously determined by the measurement of its decreased volume in the dilatometer. The penetration pressure is directly related to the sizes of the pores, according to the Washburn equation [18]:

$$R = -2\gamma \cos\theta / P_c$$

where γ is the mercury surface tension (generally 0.480 Newton / m), θ is the mercury-solid contact angle (mean value 140°), P_c is the penetration pressure and R is the pore radius. Moreover, the pore size distribution and the total porosity, together with the pore volume, can be calculated from the relation between the penetration pressure (pore size) and the penetrated mercury volume (pore volume). The hypothesis of the Washburn equation is that of cylindrical pores. Thermo Finnigan Pascal 140 and 240 porosimeters can detect pores of sizes between 58000 nm and 3.7 nm.

The porosimetry tests were executed on small samples obtained from the compression assays.

2.4.5 *The Microstructure of the Bricks*

Morphological analyses of the samples were performed using a scanning electron microscope (JEOL 5410 LV). SEM images were obtained using backscattered electrons (BSE) with an accelerating voltage of 20 kV and a beam current of 80 μA. The samples were directly introduced in the microscope sample chamber without any further treatment (like carbon or metal coating). This was possible because the used SEM-JEOL can be used in the low vacuum (LV) mode, as well as in the high vacuum mode. In the LV mode, in order to observe non-conductive specimens without conductive coating, the chamber is evacuated by a rotative pump to keep it in a low vacuum condition. Meanwhile, the electron gun chamber and lens system are evacuated by a diffusive pump to keep them in high vacuum conditions. In the low vacuum chamber, the gas molecules that surround the electron beam for specimen illumination are ionized. These charge the specimen surface and make it electrically neutralized. Thus, non-conductive specimens can be observed without coating [19].

3. Results and Discussion

In the following Figures 1, 2, 3, TEM and SEM images of the synthesized nanocrystals are reported. In Figure 1, it is possible to notice that the TiO_2 NS are made up of very fine nanocrystals, almost monodisperse, of a few nanometres in size. TiO_2 NR are a few nanometres in diameter and elongated up to about 50 nm.
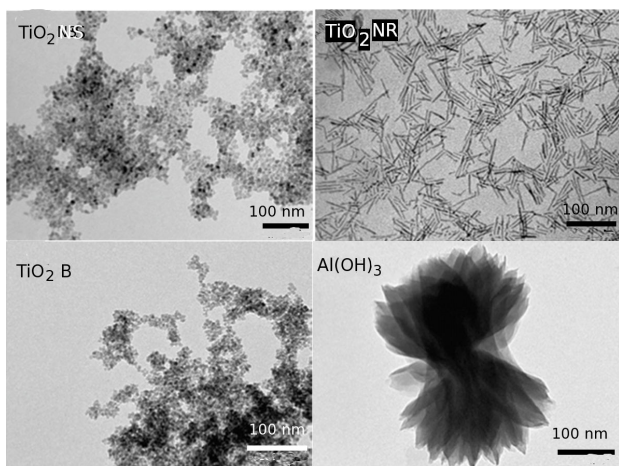
Figure 1. TEM images of the TiO$_2$ nanospheres (TiO2-NS), TiO$_2$ nanorods (TiO2-NR), TiO$_2$-boron modified (TiO2-B) (from Ref. 8) and Al(OH)$_3$ nanocrystals
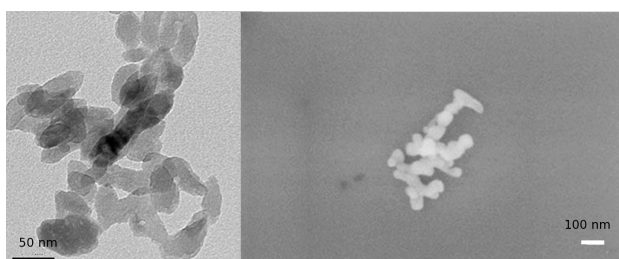

Figure 2. Images of CaCO$_3$ nanocrystals: TEM image, crystals of about 50 nm (on the left) and SEM image (on the right)

The boron modified particles TiO$_2$ B are again very fine and resemble in shape and dispersion the correspondent TiO$_2$ NS. Finally, Al(OH)$_3$ resulted in the form of "nanoflowers" with an extension of above 300 nm. The yields for microwave-assisted reactions were better than 70 % and the nanocrystals. Furthermore, according to the TEM images, the nanocrystals were almost monodispersed.
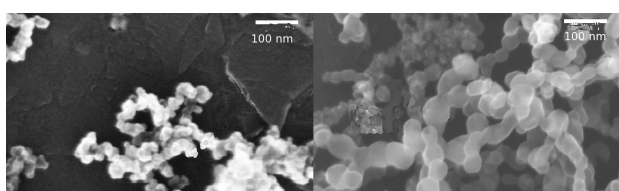

Figure 3. SEM images of SiC-16 (left panel) and SiC-28 (right panel)

In Figure 2, the CaCO$_3$ (reaction yield about 90 %) were made up of almost monodisperse grains of about 50 nm. In Figure 3, the silicon carbide SiC-16 presented aggregated grains of around 30 nm, and SiC-28 of about 50 nm. The samples differed from each other for mean size (the mean diameter of SiC-16 is 30 ± 2 nm, productivity is 15 g/h; the mean diameter of SiC-28 is 50 ± 22 nm, productivity is 50 g/h) [9], yields near 100 %. Additionally, given their shape diversity and chemical composition, their behaviour in the aluminosilicate bricks was investigated.

3.1 The Effects of the Nanocrystals Addition on the Thermo-physical and Mechanical Properties of the Aluminosilicate Bricks

Nanocrystals were added in the formulation to the commercial 55 % alumina and 42 % amorphous silica, named Vibrec 545 F. The final properties of the obtained bricks will be presented in the subsequent sections.

3.1.1 The Thermal Properties of the Nanocrystals-modified Aluminosilicate Bricks: Thermal Diffusivity

This section evaluates thermal diffusivity as a refractory parameter. It considers the heat flux under a transient regime, as described in materials and methods section.

Sample (1300 °C)	Thermal Diffusivity (mm²/s) 0.5 wt. % filler	Thermal Diffusivity (mm²/s) 1 wt. % filler	Thermal Diffusivity (mm²/s) 2 wt. % filler
Reference	1.063± 0.002	1.063± 0.002	1.063± 0.002
TiO$_2$-NS	1.045± 0.002	1.019± 0. 002	0.926± 0. 002
TiO$_2$-NR$^{(*)}$	1.032± 0. 002	1.004± 0. 002	0.989± 0. 002
TiO$_2$-B	1.000± 0. 002	0.878± 0. 002	0.840± 0. 002
Al(OH)$_3$	1.000± 0. 003	0.814± 0. 003	0.585± 0. 003
CaCO$_3$	1.083± 0. 005	1.068± 0. 005	0.916± 0. 005
SiC-16	0.894± 0. 001	0.923± 0. 001	1.099± 0. 001
SiC-28	0.975± 0. 001	0.934± 0. 001	1.034± 0. 001

Table 1. Thermal diffusivity in the nanocrystals-modified and reference aluminosilicate bricks. [*] From Ref. [8].

In Table 1, the results obtained with three different nanocrystals concentrations (0.5 wt. %, 1 wt. % and 2 wt. %) are presented and compared to the reference refractory, which were prepared without nanoparticles. All of the nanocrystals-formulated bricks presented a thermal diffusivity reduction with respect to the reference material except for SiC 16 at 2 wt. %. The trend of the fillers increasing concentration was related to a reduction in thermal diffusivity, except for SiC 16 and 28, which showed the opposite behaviour. In particular, the higher variation was obtained for 2 wt. % nano-aluminium hydroxide addition.

3.1.2 Physical Properties: Bulk and Apparent Density, Apparent Porosity and Water Absorption

The apparent and bulk densities (BD), water absorption (WA) and apparent porosity (AP) of bricks were determined via the Archimedes method using water [16]. The tests were carried out on bricks that were prepared with different nano-fillers concentrations (NFC), as well as in an unmodified brick. All of these bricks were thermally treated at 1300 °C. The obtained results, which are summarized in Table 2, showed that the nano-fillers gave a slight increase in the bulk densities with respect to the reference material, despite the fact that there was almost no correlation with the initial additives' concentrations.

Sample (1300 °C)	NFC (wt. %)	BD (g/cm³) ~ ± 0.05	AD (g/cm³) ~ ± 0.05	AP (%) ± 0.5	WA (%) ± 0.2
Ref.	-	2.70	2.28	19.0	8.3
TiO$_2$-NS	0.5	2.80	2.27	18.8	8.1
	1	2.81	2.29	18.5	8.1
	2	2.80	2.31	17.6	7.6
TiO$_2$-NR	0.5	2.82	2.29	18.6	8.1
	1	2.79	2.30	17.3	7.5
	2	2.80	2.30	18.0	7.7
TiO$_2$-B[*]	0.5	2.81	2.28	18.7	8.2
	1	2.80	2.30	18.0	7.8
	2	2.78	2.29	17.7	7.7
Al(OH)$_3$	0.5	2.81	2.23	16.6	7.6
	1	2.81	2.30	18.3	8.0
	2	2.76	2.30	20.6	9.2
CaCO$_3$	0.5	2.79	2.31	17.0	7.4
	1	2.79	2.32	17.0	7.3
	2	2.79	2.29	18.0	7.8
SiC-16	0.5	2.76	2.23	19.0	8.0
	1	2.76	2.29	17.0	7.4
	2	2.78	2.28	18.0	7.9
SiC-28	0.5	2.78	2.29	18.0	7.7
	1	2.80	2.29	18.4	8.1
	2	2.79	2.29	18.0	7.8

Table 2. Physical properties: the bulk density (BD), apparent density (AD) and porosity (AP) water absorption (WA) of nano-filled refractories. NFC – nano-filler concentration. Ref. is the reference brick. [*] From Ref. [8].

Whilst the additive concentrations were increased, there was a decrease in the apparent porosity, except for nano-Al(OH)$_3$. Therefore, most of the time, the error values were not significantly different from those of the reference brick. There was an apparent decrease in the water absorption of the modified bricks with the additive additions, except for nano-Al(OH)$_3$. Furthermore, with regard to water absorption, few values were out of the estimated error range. Given the results, such properties were not representative enough of the modification given by the nano-additives.

3.1.3 Mechanical Properties: Compression Resistance

Mechanical tests were performed once on each sample. The mechanical performances of the nanocrystals-formulated bricks were evaluated using compression breaking tests with both thermally untreated and treated reference samples.

Reference Brick	Compression Resistance (MPa)
Dried (at 105 °C)	34.0± 0.1
Treated (at 1300 °C)	80.0± 0.1

Table 3. Compression breaking resistance tests of the reference bricks

The results show that treating the bricks at 1300°C for 24 hours produced an improvement in the material compression breaking resistance (Table 3). Successively, the nanocrystals-formulated bricks, which were thermally treated, were tested for compression breaking resistance and the results are summarized in Table 4.

Sample (1300 °C)	Nano-filler Concentration (wt. %)	Compression Breaking Resistance (MPa)	Resistance Versus Concentration
Reference	-	80.0± 0.1	
TiO$_2$-NS	0.5	95.1± 0.1	
	1	98.5± 0.1	
	2	101.7± 0.1	
TiO$_2$-NR	0.5	86.2± 0.1	
	1	88.2± 0.1	
	2	97.3± 0.1	
TiO$_2$-B[*]	0.5	86.5± 0.1	
	1	88.4± 0.1	
	2	97.6± 0.1	
Al(OH)$_3$	0.5	65.4± 0.3	
	1	75.3± 0.3	
	2	89.8± 0.3	
CaCO$_3$	0.5	92.3± 0.1	
	1	95.6± 0.1	
	2	103.0± 0.1	
SiC-16	0.5	83.0± 0.2	
	1	83.9± 0.2	
	2	84.7± 0.1	
SiC-28	0.5	82.2± 0.2	
	1	83.2± 0.2	
	2	85.4± 0.2	

Table 4. Compression breaking resistance tests for all of the nanocrystals-formulated bricks, which were thermally treated at 1300 °C. Reference: brick without nanocrystals. [*]From Ref. [8].
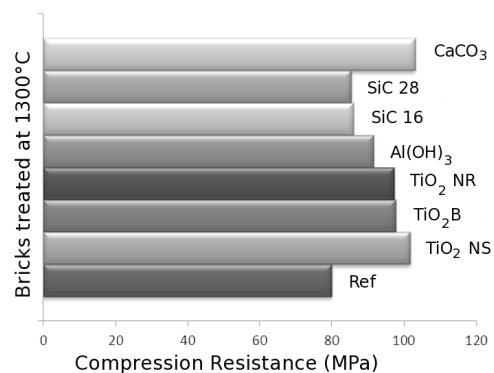

Figure 4. Comparison of compression breaking resistance for the reference (a brick without nanocrystals of commercial composition) and the different nanocrystals-formulated bricks (highest concentration: 2 wt. %) treated at 1300 °C

It was possible to deduce that the nano-additives always improved the compression breaking resistance of the refractory material with respect to reference one (Table 4).

As reported in the graphs (Table 4), the nano-filler concentration increased, as well as the compression breaking resistance.

In Figure 4, we compare the performance of the different bricks, which were thermally treated at 1300°C, with the nanocrystals (2 wt. %). The nano-fillers favoured a better refractory compaction, increasing their final compression resistance, especially after the thermal treatment. Figure 4 shows that $CaCO_3$ and TiO_2 NS gave the best performances.

3.1.4 Mercury Porosimetry Analyses

In the present section of the study, the open pore distribution and size in the refractory materials are considered.

Undoped Bricks	TCV ± 0.001 (cc/g)	SSA ± 0.01 (m²/g)	PMS ± 0.02 (μm)	TOP ± 0.06 (%)
Dried at 105 °C	0.076	1.77	0.13	18.00
Treated at 1300 °C (Reference rick)	0.098	1.45	0.35	20.84

Table 5. Porosity tests on the undoped bricks. TCV- total cumulative volume; SSA – specific surface area; PMS – pores medium size; TOP- total open porosity

The experiments, as described in the brick characterization section, were performed with a mercury porosimeter.

From the penetration curves, it is possible to take out information about the size of the pores.

At first, a brick thermally dried at 105 °C was compared with the reference brick treated at 1300 °C (Table 5, Figure 5, top graph). It is evident that there was an increase in the total cumulative volume (TCV), index of a less compact matrix of the thermally treated sample. Additionally, Table 5 shows a growth in both the total open porosity (TOP) and in the medium size pores (PMS) but with a decrement of the specific surface area (SSA).

In Table 6, data on nanocrystals-formulated samples and reference brick are resumed. The trend TCV versus the applied pressure is better presented in Figure 5. The TCV was less than in the thermally treated reference one in all the 2 % wt. Meanwhile, for the TiO_2- derived, SiC-based and $CaCO_3$-formulated bricks, it was greater in the presence of $Al(OH)_3$. In general, the SSA was greater than in the reference for all of the nanocrystals-formulated bricks, with a trend towards a SSA increase with progressive nanocrystals additions. The PMS typically had a greater response than in the reference brick, with the trend of increasing values with the progressive addition of nanocrystals.

Therefore, the PMS was obtained on the basis of the Washburn hypothesis of cylindrical pores. With the exception of $Al(OH)_3$, the TOP was less than for the reference. Furthermore, for all of the fillers, it increased with the concentrations.
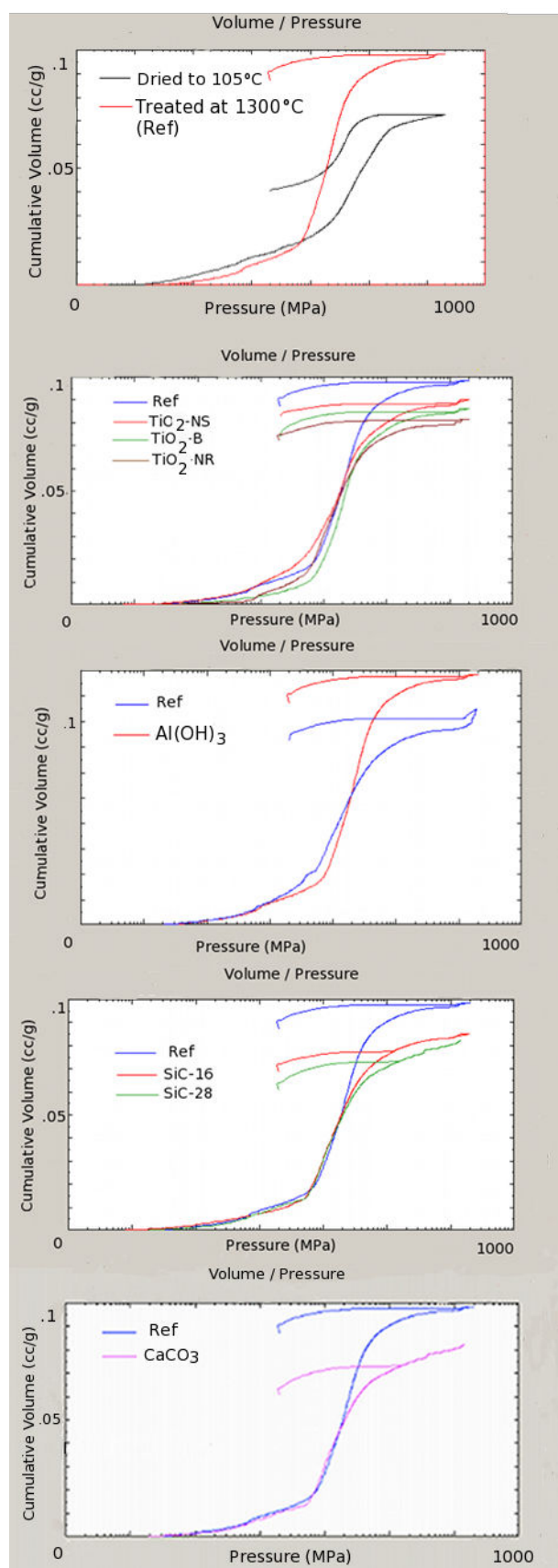

Figure 5. Cumulative infiltration volume versus applied pressure (2 % wt. thermally treated samples). In the figure, Ref stands for the commercial brick without nanocrystals and thermally treated at 1300 °C.

Sample	NFC (wt. %) ± 0.001	TCV ± 0.001 (cc/g)	SSA ± 0.01 (m²/g)	PMS ± 0.02 (μm)	TOP ± 0.06 (%)
Reference	-	0.098	1.45	0.35	20.84
TiO$_2$-NS	0.5	0.082	1.47	0.36	17.97
	1	0.084	1.48	0.43	18.70
	2	0.090	1.71	0.50	19.33
TiO$_2$-NR	0.5	0.080	1.47	0.87	17.54
	1	0.080	1.50	0.90	17.60
	2	0.081	1.52	0.93	17.67
TiO2-B$^{(*)}$	0.5	0.083	1.49	0.36	19.77
	1	0.085	1.53	0.45	19.82
	2	0.086	1.58	0.50	19.94
Al(OH)$_3$	0.5	0.086	2.34	0.85	21.50
	1	0.090	3.64	0.98	22.30
	2	0.100	4.03	1.02	22.70
CaCO$_3$	0.5	0.081	1.46	0.56	19.25
	1	0.082	1.48	0.60	19.46
	2	0.085	1.50	0.61	19.54
SiC-16	0.5	0.072	1.45	0.60	18.61
	1	0.082	1.45	0.64	18.76
	2	0.085	1.48	0.68	18.89
SiC-28	0.5	0.083	1.66	0.73	17.69
	1	0.083	1.75	0.76	17.87
	2	0.082	1.80	0.78	18.00

Table 6. Comparison porosity test among the reference brick and the nanocrystals-formulated bricks (all of which were thermally treated at 1300 °C): NFC – nano-filler concentration. $^{(*)}$ From Ref. [8]. TCV- total cumulative volume; SSA – specific surface area; PMS – pores medium size; TOP- total open porosity.

3.1.5 Morphological SEM Analyses

The morphology of the reference material (a brick thermally treated at 1300 °C and without nanocrystals) and nanocrystals-formulated bricks was investigated using a scanning electron microscopy. The samples were fractured under liquid nitrogen.
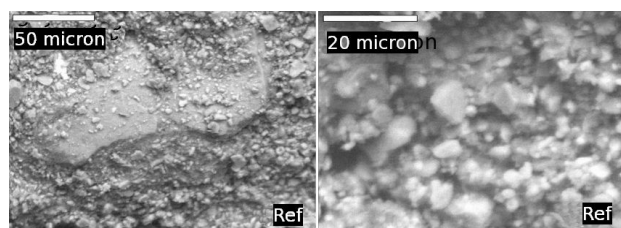

Figure 6. SEM micrographs of the reference brick, thermally treated at 1300 °C

The images relate to the fractured surface. Figure 6 shows the reference sample thermally treated at 1300 °C.

It was possible to notice a coarse material structure. At higher magnification (right panel), the microstructure was heterogeneous, with noticeable diameter grains besides the finer particles. Texture modifications in the mixture during the thermal treatment are principally due to sintering, which determines the structure consolidation following the
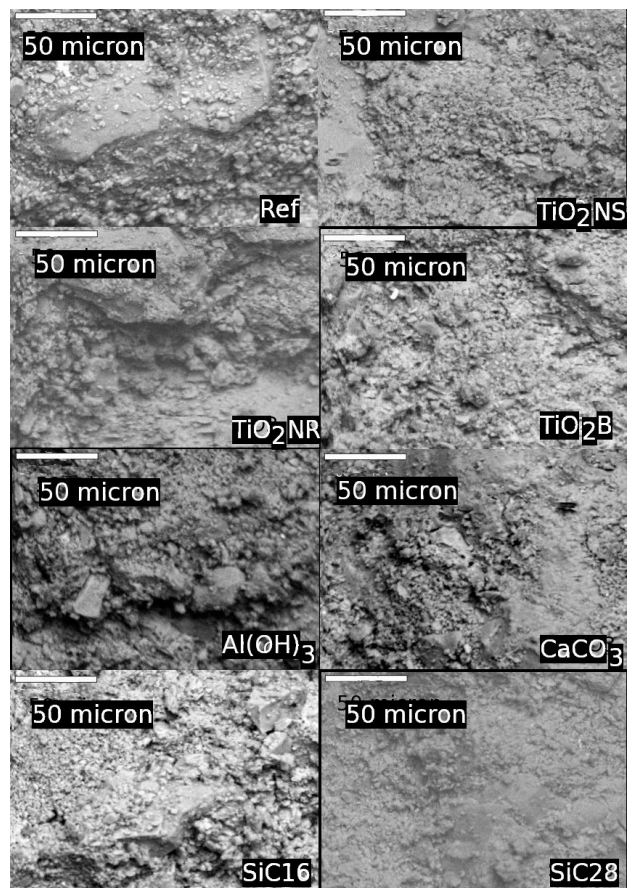

Figure 7. Comparative SEM micrographs of the nanocrystals-formulated (2 wt. %) and the reference (without nanocrystals additions) bricks, all thermally treated at 1300 °C. TiO$_2$ B. From Ref. [8].

coalescence of particles, even below their fusion point. This process takes place by diffusion at temperatures that depend principally on the type of material and on the redox condition of the atmosphere during the heating process.

In Figure 7, SEM images of the thermally treated nanocrystals-formulated 2 wt. % bricks are reported.

At first inspection, the presence of smooth and particularly rough zones were observed. The latter was due to the sample preparation procedure. From the shown SEM images, it was not possible to finely evaluate the differences in porosity.

4. Conclusions

In the present work, the results regarding the thermo-physical and mechanical characterization of the nanocrystals-formulated aluminosilicate refractories are presented. The matrix is made of a commercial aluminosilicate (55 % Al$_2$O$_3$, 42 % SiO$_2$). Different synthesized nanocrystals were added to it to prepare the bricks, with the aim to obtain an improvement in heat-insulating and/or mechanical refractory properties.

All of the samples, according to international norms, were thermally treated at 1300 °C for 24 hours.

Each kind of nanocrystal-filled refractory was prepared with the addition of three different benzyl alcohol suspensions of nanoparticles in 0.5 wt. %, 1 wt. % and 2 wt. % amounts in the mixture to avoid agglomeration of the nanoparticles.

Under the errors, the investigated physical properties, such as the bulk and apparent density, apparent porosity and water absorption, were not able to produce results that were significant enough to work out the relationship between the concentrations of nano-additives and bricks.

The thermal diffusivities correlated with the amount of nanocrystals. With the increasing concentrations, their reductions were registered, except for SiC-16 and SiC-28, which showed an opposite trend; 2 % wt. nano-$Al(OH)_3$ resulted in the best performing heat-insulating material. All of the other nanocrystals-formulated bricks, with the exception of the SiC-based ones, presented a decrement of thermal diffusivities with respect to the reference material. Nano-$Al(OH)_3$ was confirmed by mercury porosimetry as the best additive to induce increasing TCV, SSA, PMS and TP. Air in the pores could explain the lower heat transfer performances. For the other nanocrystals, the comparison of the porosimetry tests with the thermal conductivities results was less straightforward. This is most probably because other factors, rather than only porosity, played a relevant role.

The mechanical tests showed an improvement in resistance with respect to the reference brick with all of the tested nanocrystals additives, according to their increasing concentrations. It is likely that benzyl alcohol alone could also have played a role, especially on the pores. However, this effect was not tested in an ad hoc prepared reference brick. In fact, pores can be easily generated during the heat treatment via organic inclusions. Among the synthesized particles, TiO_2 NS resulted (from Raman analysis) in a surface that was functionalized with acetate, TiO_2 NR with oleate and $Al(OH)_3$ with acetate, which may have played a role. Nano-$CaCO_3$ and TiO_2 NS at the highest 2 wt. % concentrations showed the best mechanical resistance performances.

Therefore, to be sure that the properties of the bricks were due to the nanoscale state of the added particles, further experiments should be performed with micrometric particles of the same composition in brick formulation. The syntheses adopted were studied for the production of nanometric particles. Thus, it could be possible that they are not suitable for the production of micrometric particles. The effect of particle size on the final properties of the bricks is still an open issue.

Moreover, the bricks were thermally threated at 1300 °C for 24 hours and the nanocrystals were not protected against reactions with the matrix and decomposition or thermally induced transformations. Thus, the final product would not be a nanocomposite, like the starting material, but rather, a ceramic material.

It is possible that the nano-sized state of the added fillers may have induced the relevant local modifications in the matrix. This may have influenced the porosity and the characteristics of the pores during the thermal treatments. However, as it was previously stated, the nanosize dependency could not be demonstrated at this stage.

6. References

[1] Sobolev K, Gutiérrez M F (2005) How Nanotechnology Can Change the Concrete World. American Ceramic Society Bulletin 84: 14-18.

[2] Nazari A, Riahi S, Riahi S, Shamekhi S F, Khademno A (2010) Improvement the Mechanical Properties of the Cementitious Composite by Using TiO_2 Nanoparticles. Journal of American Science 6: 98-101.

[3] Jiraborvornpongsa N, Imai M Yoshida K, Yano T (2013) Effects of Trace Amount of Nanometric SiC Additives with Wire or Particle Shapes on the Mechanical and Thermal Properties of Alumina Matrix Composites. J. Mater. Sci. 48: 7022–7027.

[4] Wang H Z, Gao L, Guo J K (2000) The Effect of Nanoscale SiC Particles on the Microstructure of Al_2O_3 Ceramics. Ceramics International 26: 391-396.

[5] Sciti D, Vicens J, Bellosi A (2002) Microstructure and Properties of Alumina-SiC Nanocomposites Prepared from Ultrafine Powders. J. Mater. Sci. 37: 3747–3758.

[6] Carlucci C, Xu H, Scremin B F, Giannini C, Altamura D, Carlino E, Videtta V, Conciauro F, Gigli G, Ciccarella G (2014) Selective Synthesis of TiO_2 Nanocrystals with Morphology Control with the Microwave-solvothermal Method. Cryst. Eng. Comm. 16: 1817-1824.

[7] Carlucci C, Xu H, Scremin B F, Giannini C, Sibillano T, Carlino E, Videtta V, Gigli G, Ciccarella G (2014) Controllable One-pot Synthesis of Anatase TiO_2 Nanorods with the Microwave-solvothermal Method. Sci. Adv. Mat. 6: 1-8.

[8] Carlucci C, Conciauro F, Scremin B F, Antico A G, Muscogiuri M, Sibillano T, Giannini C, Filippo E, Lorusso C, Congedo P M, Ciccarella G (2015) Properties of Aluminosilicate Refractories with

Synthesized Boron-modified TiO_2 Nanocrystals. Nanomater. Nanotechnol. 5:8.

[9] D'Amato R, Falconieri M, Gagliardi S, Popovici E, Serra E, Terranova G, Borsella E (2013) Synthesis of Ceramic Nanoparticles by Laser Pyrolysis: from Research to applications. Journal of Analytical and Applied Pyrolysis 104: 461-469.

[10] Ciccarella G, Vergaro V, Leporatti S, Patent N. EP13425061. Synthesis of $CaCO_3$ Nanoparticles by Means of Spray Dryer.

[11] UNI EN 196, Norms under the Website http://www.uni.com/ Italian Organization for Standardization. Accessed 2014 September 22.

[12] FULLPROF Refinement of Powder (Rietveld) and Single Crystal Diffraction Data http://ill.eu./sites/fullproff. Accessed 2014 September 22.

[13] Xu H, Picca R A, De Marco L, Carlucci C, Scrascia A, Papadia P, Scremin B F, Carlino E, Giannini C, Malitesta C, Mazzeo M, Gigli G, Ciccarella G (2013) Nonhydrolytic Route to Boron-doped TiO_2 Nanocrystals. Eur. J. Inorg. Chem. 2013(3): 364–374.

[14] Gustafsson S E (1991) Transient Plane Source Techniques for Thermal Conductivity and Thermal Diffusivity Measurements of Solid Materials. Rev. Sci. Instrum. 62: 797.

[15] Log T, Gustafsson S E (1995) Transient Plane Source (TPS) Technique for Measuring Thermal Transport Properties of Building Materials. Fire and Materials 19: 43-49.

[16] American Society for Testing and Materials. www.astm.org. Accessed 2014 September 22.

[17] Carlos A, Léon y Léon (1998) New perspectives in Mercury Porosimetry. Advances in Colloid and Interface Science 76-77: 341-372.

[18] Washburn E W (1921) The Dynamics of Capillary Flow. Phys. Rev. 17: 273-283.

[19] Donald A M (2003) The Use of Environmental Scanning Electron Microscopy for Imaging Wet and Insulating Materials. Nat. Mater. 2: 511-516.